

Multiband Photopolarimetric Monitoring of the Outburst of the Blazar 3C 454.3 in 2007

Mahito SASADA¹, Makoto UEMURA², Akira ARAI³, Yasushi FUKAZAWA¹, Koji S. KAWABATA²,
Takashi OHSUGI², Takuya YAMASHITA⁴, Mizuki ISOGAI³, Osamu NAGAE¹, Takeshi UEHARA¹,
Tsunefumi MIZUNO¹, Hideaki KATAGIRI¹, Hiromitsu TAKAHASHI¹, Shuji SATO⁵, and Masaru KINO⁵

¹*Department of Physical Science, Hiroshima University, Kagamiyama 1-3-1, Higashi-Hiroshima 739-8526*
sasada@hep01.hepl.hiroshima-u.ac.jp

²*Astrophysical Science Center, Hiroshima University, Kagamiyama 1-3-1, Higashi-Hiroshima 739-8526*

³*Faculty of Science, Kyoto Sangyo University, Motoyama, Kamigamo, Kita-Ku, Kyoto-City 603-8555*

⁴*National Astronomical Observatory of Japan, Osawa, Mitaka, Tokyo 181-8588*

⁵*Department of Physics, Nagoya University, Furo-cho, Chikusa-ku, Nagoya 464-8602*

(Received 2009 December 23; accepted 2010 March 9)

Abstract

We report on optical—near-infrared photopolarimetric observations of a blazar 3C 454.3 over 200 d. The object experienced an optical outburst in July 2007. This outburst was followed by a short state fainter than $V = 15.2$ mag lasting ~ 25 d. The object, then, entered an active state during which we observed short flares having a timescale of 3–10 d. The object showed two types of features in the color–magnitude relationship. One is a “bluer-when-brighter” trend in the outburst state, and the other is a “redder-when-brighter” trend in the faint state. These two types of features suggest a contribution of a thermal emission to the observed flux, as suspected in previous studies. Our polarimetric observation detected two episodes of the rotation of the polarization vector. The first one was a counterclockwise rotation in the QU plane during the outburst state. After this rotation event of the polarization vector, the object entered a rapidly fading stage. The second one was seen in a series of flares during the active state. Each flare had a specific position angle of polarization, and it apparently rotated clockwise from the first to the last flares. Thus, the object exhibited rotations of the polarization vector in opposite directions. We estimated a decay timescale of the short flares during the active state, and then calculated an upper limit of the strength of the magnetic field, $B=0.2$ G, assuming a typical beaming factor of blazars, $\delta = 20$. This upper limit of B is smaller than those previously estimated from spectral analysis.

Key words: BL Lacertae Objects: individual: 3C 454.3 — polarization — infrared: general

1. Introduction

Blazars are a subclass of active galactic nuclei (AGN), in which a relativistic jet is viewed at a small angle to the line of sight. They comprise two groups of objects, BL Lac objects and Flat Spectrum Radio-loud Quasars (FSRQs). Emission lines which originates from the nuclear region (broad and narrow line regions) are observable in the optical range in FSRQs, and rarely in BL Lac objects (Urry & Padovani 1995).

The radio and optical fluxes from blazars are highly polarized because synchrotron radiation from jets is dominant in the radio—optical bands. Since the polarization can be a probe of the magnetic field in the jet, observations of temporal variations of polarization are important for the investigation of the structure of the jet. Rotations of polarization vectors have, in particular, attracted attentions (e.g. Qian et al. 1991; Sillanpää et al. 1993). Jones et al. (1985) proposed that an apparent rotation is a result of random motion of the polarization vector. Marscher et al. (2008) have recently reported a smooth rotation of the polarization vector associated with an optical flare in BL Lac. They proposed that the rotation cannot be ex-

plained by the random motion scenario, and indicates an emitting zone passing through a helical magnetic field. The timescale of the rotation event in BL Lac is so short (~ 5 d) that a number of similar events might have been missed before. Larionov et al. (2008) reported that the polarization vector in 3C 279 had rotated smoothly over approximately two months. And another rotation event in PKS 1510–089 was reported by Marscher et al. (2010), lasting 50 ± 10 d. Long-lasting and high time-resolved polarimetric observations are required to determine whether observed rotations indicate real structures of the magnetic field in jets.

3C 454.3 is classified as a FSRQ. Raiteri et al. (2007) and Raiteri et al. (2008) reported a UV excess over the synchrotron component in the spectral energy distribution (SED). The UV excess suggests a substantial contribution of the thermal emission from an accretion disk. Until ~ 2001 only a moderate variability in a range of $R \sim 15 - 17$ mag was observed in the optical regime (Villata et al. 2006). The object showed an unprecedentedly bright optical outburst in May 2005. Fuhrmann et al. (2006) reported that the object reached a maximum about $R \sim 12.0$ mag during this bright outburst. The ob-

ject again experienced a major outburst in July—August 2007, and subsequently another short flares in November 2007—February 2008 (Raiteri et al. 2008). The object reached a maximum of $R = 12.58$ mag during the outburst state in 2007. In the gamma-ray region, a flare was also detected by the AGILE satellite together with the 2007 optical outburst (Vercellone et al. 2008).

In general, a blazar becomes bluer when it is brighter. This feature is so-called the “bluer-when-brighter” trend (e.g. Racine 1970). On the other hand, a “redder-when-brighter” trend has been observed in 3C 454.3 (Miller 1981; Villata et al. 2006; Raiteri et al. 2007). This trend showed a “saturation” at $R \sim 14$ mag, and the object possibly turned into a bluer-when-brighter trend in the bright states during the 2007 outburst (Raiteri et al. 2008). The redder-when-brighter trend in 3C 454.3 is probably caused by a substantial contribution of the thermal emission from the disk. Simultaneous optical and near-infrared (NIR) observations could detect the bluer-when-brighter trend in the bright state more clearly than the observations only within the optical regime.

We performed photopolarimetric observations of 3C 454.3 simultaneously in the optical and NIR bands from July 2007 to February 2008. In this paper, we report the light curve, color and polarization variations of 3C 454.3 in the optical and NIR regions. Our polarimetric observations found intriguing rotations of the polarization vector. This paper is arranged as follows: In section 2, we present the observation method and analysis. In section 3, we report the result of the photometric and polarimetric observations. In section 4, first, we discuss the origin of a long term component under the short flares. Second, we discuss implications of the observed rotation events of the polarization vector. Finally, we estimate the strength of magnetic field using a decay timescale of flares. The conclusion is drawn in section 5.

2. Observation

We performed monitoring of 3C 454.3 from July 18, 2007 to February 2, 2008 using TRISPEC attached to the Kanata 1.5-m telescope at Higashi-Hiroshima Observatory. TRISPEC (Triple Range Imager and SPECTrograph) has a CCD and two InSb arrays, enabling photopolarimetric observations in an optical and two NIR bands simultaneously (Watanabe et al. 2005). We used the photopolarimetric mode of TRISPEC with V -, R_C -, I_C -, J -, and K_S -band filters. Although we obtained the polarimetric observation data in all bands, we report the polarization parameter only in the V band in this paper. The data in the V , J and K_S bands were observed in the entire period. The data in the R_C and I_C bands were obtained from JD 2454428 to 2454440. A unit of the observing sequence consisted of successive exposures at four position angles of a half-wave plate; 0° , 45° , 22.5° , 67.5° . A set of polarization parameters was derived from each set of the four exposures.

Integration time in each exposure varied night by night, depending on the sky condition and the brightness of

3C 454.3. Typical integration times were 90, 108, 108, 85 and 70 s in the V , R_C , I_C , J and K_S bands, respectively.

All images were bias-subtracted and flat-fielded, and we performed aperture photometry with the *IRAF APPHOT* package. We performed differential photometry with a comparison star taken in the same frame of 3C 454.3. Its position is R.A.= $22^{\text{h}}53^{\text{m}}58^{\text{s}}11$, Dec.= $+16^\circ09'07''.0$ (J2000.0) and its magnitudes are $V = 13.587$, $R_C = 13.035$, $I_C = 12.545$, $J = 11.858$ and $K_S = 11.241$ mag (González – Pérez et al. 2001; Skrutskie et al. 2006). The comparison star is listed in Fiorucci et al. (1998) as star H. The position of a check star is R.A.= $22^{\text{h}}53^{\text{m}}44^{\text{s}}63$, Dec.= $+16^\circ09'08''.1$ listed in González – Pérez et al. (2001) as star 14. Using the check star, we confirmed that the comparison star was almost constant in magnitude within 0.05 mag during our observation period. We calculated the magnitude of 3C 454.3 using another neighboring stars listed in González – Pérez et al. (2001), and estimated a systematic error of the magnitude of 3C 454.3 depending on the comparison stars to be ~ 0.1 mag in all photometric bands. In this paper, the error of the flux of 3C 454.3 in figure 6 includes both the systematic and photon statistical errors, and that in the other figures includes only the photon statistical error.

We confirmed that the instrumental polarization was smaller than 0.1 % in the V band using the observation of unpolarized standard stars. We, hence, applied no correction for it. The zero point of the polarization angle is corrected as the standard system (measured from north to east) by observing the polarized stars, HD 19820 and HD 25443 (Wolff, Nordsieck & Nook 1996).

3. Result

3.1. Optical and NIR light curves

Figure 1 shows the light curve in the V band, the color variations in $V - K_S$ and $V - J$. We also show the relative magnitude, C1-C2, between the comparison star (C1) and the check star (C2). We can recognize three states of the object based on the temporal behavior; the first is an outburst state from JD 2454300 to 2454350, the second is a faint state from JD 2454350 to 2454374, and the last is an active state from JD 2454374 to 2454500.

According to Raiteri et al. (2008), the outburst started on \sim JD 2454270, and reached a maximum of $R \sim 12.7$ mag in JD 2454300. We found $V \sim 13.2$ mag on the same night (when we started our monitoring). After the maximum, we detected a short fading, which was followed by a rebrightening trend. Several short flares were superimposed on the rebrightening trend, for example on JD 2454326 and 2454334. The object exhibited a rapid fading from the outburst state from JD 2454345, and then became faint to $V = 15.2$ mag within 10 d.

In May 2005, the object experienced an exceptionally large outburst (Fuhrmann et al. 2006). The object reached a maximum about $V = 12.7$ and $R = 12.2$ mag. In the case of the 2005 outburst, it took ~ 75 d to decay from the outburst maximum to the faint state of $R = 15.8$ mag

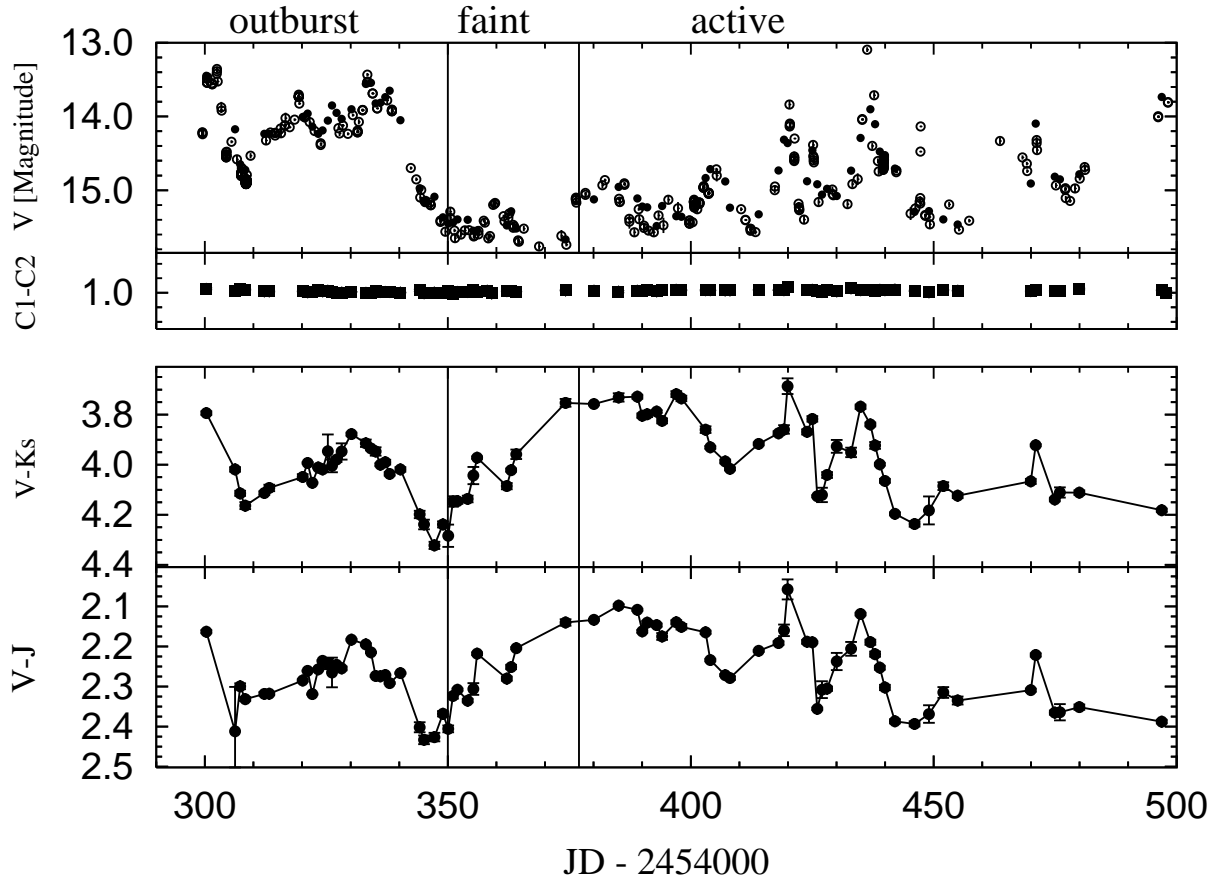


Fig. 1. Light curve of 3C 454.3 in the V band, color variations of $V - K_S$ and $V - J$. The filled and open circle denote the observation with the Kanata telescope and by the WEBT team, respectively. We also show the relative magnitude, C1-C2, between the comparison star (C1) and the check star (C2). The three states, that is, “outburst”, “faint” and “active” states, can be defined as indicated by the vertical solid lines (for detail, see the text).

(Villata et al. 2006). The 2005 outburst, thus, faded much more slowly than the 2007 outburst.

After the rapid fading of the 2007 outburst, the object entered the faint state lasting 25 d. The criterion between the outburst and faint states is also based on different color–magnitude relationships, as reported in subsection 3.2. The object was relatively inactive in the V band, showing no significant variation over 0.6 mag during the faint state.

3.2. Color Variation

Figure 2 shows the color–magnitude relationships in the outburst (top panel), the faint (middle panel) and the active states (bottom panel). In the outburst state, the color well correlated with the V -band flux both in the long outburst trend and the short flares superimposed on the outburst. The object exhibited a bluer-when-brighter trend. A rapid reddening was associated with the rapid fading from the outburst. At the beginning of the faint state, the object was reddest during our observation period.

The color–magnitude relationship in the faint state is totally different from that in the outburst state, as clearly

shown in figure 2. The V -band flux kept a slow decline in the faint state, although the color showed a rapidly bluing trend. In contrast to the outburst state, the faint state showed a redder-when-brighter trend.

In the active state, a bluer-when-brighter trend was associated with the short flares. The object was quite bright both on JD 2454300 and 2454498. The color on JD 2454498 was, however, significantly redder than that on JD 2454300, as can be seen in figure 1. This color behavior suggests the presence of a long-term reddening trend during the active state. The color–magnitude relation in the active state is apparently complex compared with those in the outburst and faint states, as shown in figure 2. This can be interpreted as a result of the superposition of two components, namely the short flares with a bluer-when-brighter trend and the long term component with a reddening trend.

Raiteri et al. (2007) reported the presence of a thermal component in the SED of 3C 454.3. The redder-when-brighter trend of 3C 454.3 in the faint state is, hence, interpreted as the increase of the contribution of the synchrotron emission compared with the thermal emission,

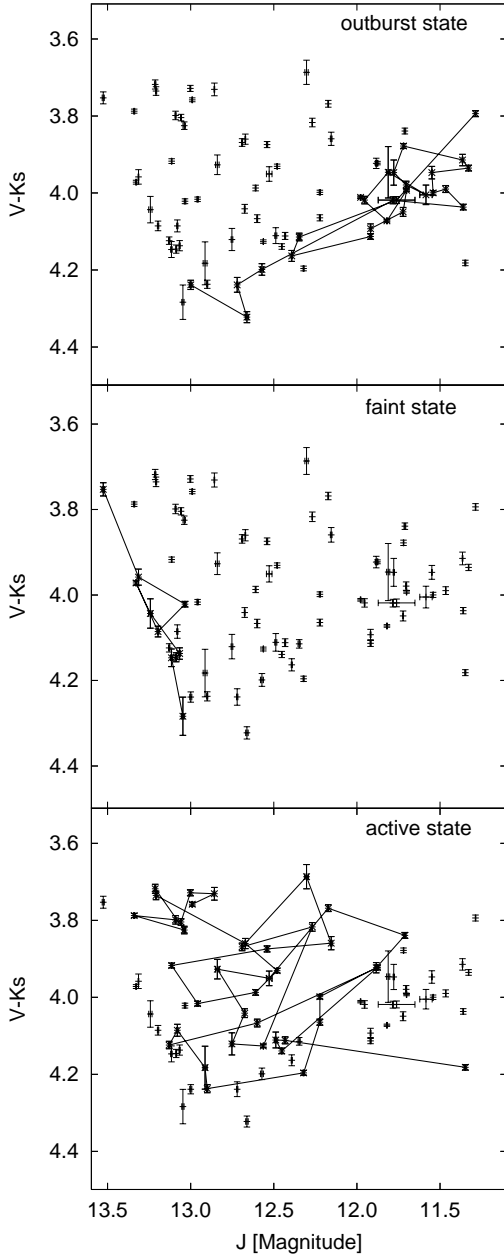


Fig. 2. Color–magnitude diagram in the J -band magnitude and $V - K_S$ color. The outburst, faint and active states are indicated by the solid lines connecting the observed points in the top, middle and bottom panels, respectively.

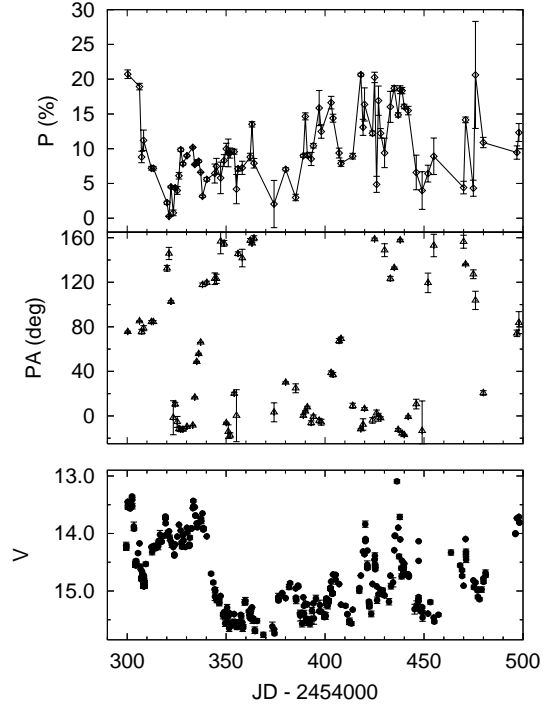


Fig. 3. Temporal variation of the polarization of 3C 454.3; (Top) polarization degree (%) in the V band, (middle) polarization angle (degree) in the V band, and (bottom) V -band light curve. We set the range of the polarization angle from -20° to 160° .

when the flux increased. The reddening feature of the long term component in the active state suggests that the contribution of the synchrotron emission increased with time.

Raiteri et al. (2008) reported on the $B - R$ color variation associated with the flux variation between 2005–2008. In their observation, 3C 454.3 generally exhibited a redder-when-brighter trend, while the trend weakened when the object was brighter than $R \sim 14$ mag. The color behavior obtained by our observations is generally consistent with that reported in Raiteri et al. (2008), except for the clear bluer-when-brighter trend detected in our observation. We propose two reasons why the bluer-when-brighter trend was prominent in our observations. One reason is that the contribution of the synchrotron emission is larger in the NIR region than in the optical. The other is that the range of wavelength between V and J bands are larger than that between B and R bands. An observation with a wider range of the wavelength would detect a small color-variation more readily.

3.3. Polarization parameters

Figure 3 shows the temporal variation of the polarization degree (top), the polarization angle (middle) and the light curve (bottom) in the V band. Figure 4 shows temporal variations of the polarization vector in the QU planes. The observed flux was corrected for the interstellar absorption in our Galaxy in the middle and bottom

panels of figure 4 (Schlegel, Finkbeiner & Davis 1998). The V -band light curve is shown in the top panel of figure 4 just for reference. In the middle and bottom panels, the points during the outburst and the active states are connected with the solid and dashed lines, respectively. We calculated Stokes parameters Q and U using the energy flux, $I (= \nu F_\nu)$, and Q/I and U/I obtained from the observation.

The polarization degree was quite high ($20.7 \pm 0.6\%$) in the early outburst state, then rapidly decreased to almost 0% within 21 d. The polarization vector subsequently showed a smooth counterclockwise rotation in the QU plane, as shown in the middle panel of figure 4. This rotation episode lasted for 19 d from JD 2454328. The rotation speed was fairly constant with $dPA/dt = 22 \pm 3$ degree/d particularly from JD 2454333 to 2454338. It is evidently difficult to explain this systematic rotation by a result of a random walk in the QU plane (Jones et al. 1985). The object entered the rapid fading stage from the outburst after that rotation of the polarization vector.

Another rotation episode of the polarization vector was observed during the active state. We labeled six flares in the active state from “A” to “F”, as indicated in the top and bottom panels of figure 4. We calculated the averages of Q and U during each flare, which is indicated by the open diamonds in the bottom panel. The filled square in the bottom panel denotes the averages of Q and U of the bottom of the flares. The averages of Q and U in each flare were significantly apart from those of the bottom of the flares, except for flare A. The directions of polarization were different in flare by flare. Our observation, thus, indicates that a specific polarization vector was associated with those flares. Furthermore, the average polarization angles of the flares apparently rotate in a clockwise direction from the first to the last.

The first counterclockwise rotation in the outburst state is analogous to the rotation which has recently been observed in BL Lac in terms of the timescale and the smoothness of the variation in the polarization angle (Marscher et al. 2008). The second clockwise rotation was an unprecedented event in which a flare-by-flare rotation was observed. This is also the first time that the two rotations of the polarization vector were consecutively observed, and furthermore, in opposite directions.

As well as the increase of the polarized flux, the increase of the polarization degree was likely to be associated with the short flares in the active state, as can be seen in figure 3. On the other hand, no such a trend can be seen for the long-term reddening component in the active state. For example, the polarization degrees in \sim JD 2454500 were comparable with those of the bottoms of the short flares in JD 2454400–2454430, while the total flux was much higher in \sim JD 2454500 than that in the short flare in JD 2454400–2454430.

3.4. Temporal variation of the spectral energy distribution associated with a short flare

We performed V -, R_C -, I_C -, J -, K_S -band photometry during the short flare “E”. In this section, we report the

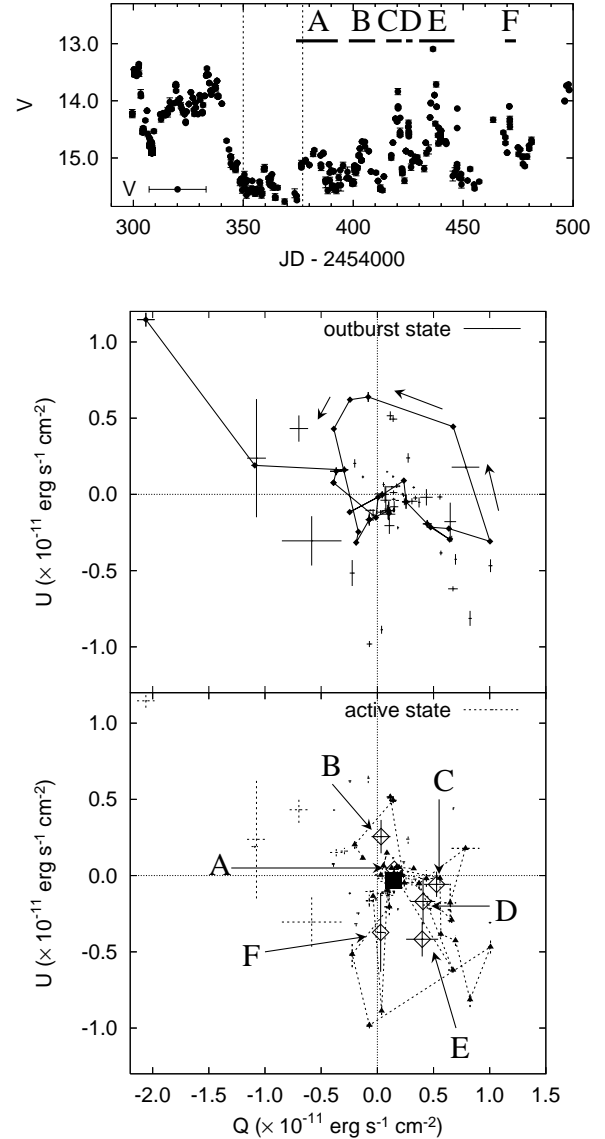


Fig. 4. Top panel: Light curve of the object in the V band. The period of the outburst, faint, and active states were indicated by the vertical dashed lines. In the active state, we identified 6 flares, that is, flare A (from JD 2454374 to 2454393), B (from JD 2454398 to 2454408), C (from JD 2454413 to 2454423), D (from JD 2454424 to 2454427), E (from JD 2454430 to 2454446) and F (from JD 2454470 to 2454475). Middle panel: The QU plane during the outburst state in the V band. Bottom panel: The QU plane during the active state in the same band. The open squares indicate the averaged QU points during each flare. The flux was calculated with $1.98 \times 10^{-5} \text{ erg sec}^{-1} \text{ cm}^{-2}$ at 0 mag in V band (Fukugita et al. 1995)

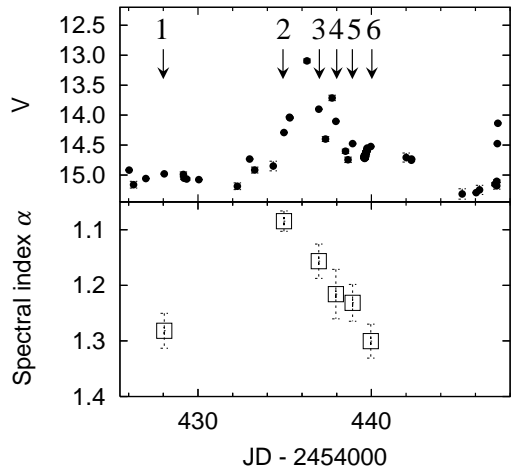


Fig. 5. Upper panel: Light curve of flare “E” in the V band. The labels from 1 to 6 indicate the epochs in which we performed 5-band multicolor observations. Lower panel: Temporal variation of spectral index α from epoch 1 to 6.

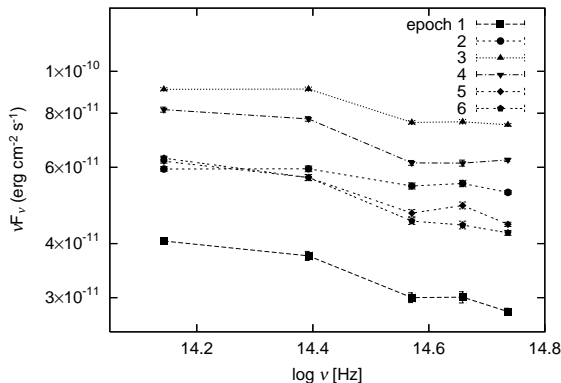


Fig. 6. SEDs from the V to the K_S bands at each epoch. The vertical axis indicates the flux, and the unit is $\text{erg sec}^{-1} \text{cm}^{-2}$. These fluxes were calculated with 1.42, 0.895, 0.384 and $0.0867 \times 10^{-5} \text{erg sec}^{-1} \text{cm}^{-2}$ at 0 mag in R_C , I_C , J and K_S bands, respectively (Fukugita et al. 1995 and Bessell, Castelli & Plez 1998).

temporal variation of the SED during this flare.

The upper and lower panels of figure 5 show the V-band light curve and the temporal variation of the spectral index during flare “E”, respectively. Six epochs from 1 to 6 are indicated, in which the 5-band photometric data are available. We calculated the spectral index, α , using the 5-band absorption-corrected data, assuming a power-law form of SEDs, that is, $F_\nu \propto \nu^{-\alpha}$. In order to ignore fine structures of the spectra, we fitted the data with errors of 10 % of the flux. Epoch 2 was in a rising phase of the flare. Epoch 3, 4, 5 and 6 were in a decay phase.

As can be seen in figure 5 and 6, the epoch with

the hardest SED precedes the peak of the V-band flux. Takahashi et al. (1996) reported the X-ray spectral evolution associated with a flare of Mrk 421 whose timescale is similar to that of flare “E” in 3C 454.3. According to Takahashi et al. (1996), the X-ray spectrum was hardest before the flare maximum, as observed in our optical—NIR observations of 3C 454.3. Mrk 421 is one of objects called as high frequency BL Lac objects, in which the synchrotron peak frequency is in the X-ray range. On the other hand, the synchrotron peak frequency of 3C 454.3 is in the infrared range. The SED evolutions of the synchrotron flares are remarkably analogous in Mrk 421 and 3C 454.3, although the peak frequencies of the synchrotron radiation are totally different.

4. Discussion

4.1. Long term component during the active state

We found distinct two components during the active state, namely, the short flares and the long-term reddening component. The flares in the active state had short timescales, the bluer-when-brighter trend and specific polarization components. Compared with these features of the flares, the long term component had a long timescale, reddening trend and no correlation of the polarization degree.

The size of the emitting zone of the long term component would be larger than that of the short flares if the observed timescale represents the light travel time of the emitting zone. The observed behavior of polarization may be interpreted with the difference in the emitting region size. The magnetic field in various directions possibly exists in a large emitting area. In this case, the polarization of a certain area is diluted by those of another areas, and thereby, the polarization degree may be insensitive to the flux variation, as observed in the long term component. On the other hand, the direction of the magnetic field is expected to be relatively ordered in a small, or local area. Flares from such a small area would be observed with an increase of the polarization degree, as the short flares in the active state.

4.2. Rotations of the polarization vector

The object exhibited two episodes of polarization-vector rotations both in the clockwise and counterclockwise directions in the QU plane. Marscher et al. (2008) proposed that the rotation of the polarization vector occurs when the optical emitting zone propagates outward along a helical magnetic field in the jet. As mentioned in subsection 3.3, the rotation of the polarization vector in the outburst state in 3C 454.3 is reminiscent of that in BL Lac observed by Marscher et al. (2008). In the case of the clockwise rotation in the active state, the emitting zone should shift to inverse direction compared with the counterclockwise rotation in the outburst, if the scenario proposed in Marscher et al. (2008) is applied to our result. In other words, our results require both outward and inward shifts of the emitting zone in the jet. However, it is difficult to consider an upstream propagation of a shock

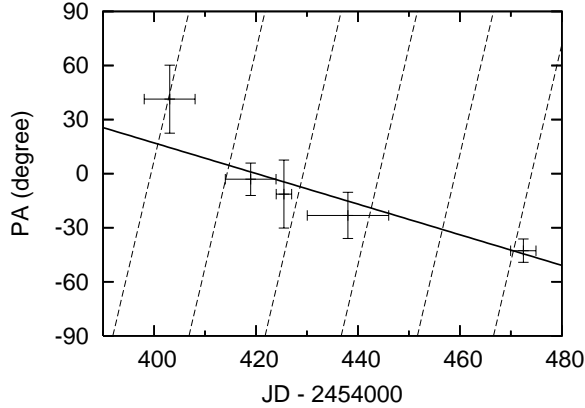


Fig. 7. Temporal variation of the polarization angle of the short flares during the active state. The solid line shows the best-fitted model of the clockwise rotation. The dashed line shows that of counterclockwise rotation.

or emitting matter in the jet. An apparent inward shift of the emitting zone may be possible if the location of the emitting zone systematically varies depending on the physical condition in the jet. For example, if the dominant emitting zone locates in the downstream of the jet during an outburst, the emitting zone can apparently shift to the upstream as the outburst finishes. If this is the case for 3C 454.3, similar rotations of the polarization vector should be confirmed in every outbursts.

We can consider an alternative scenario that the polarization vector actually rotated in the counterclockwise direction in the active state, because the observed polarization angle has an ambiguity of 180 degree. In the outburst state, the rotation rate of the polarization angle was 22 degree/d as mentioned subsection 3.2. Figure 7 shows the temporal variation of the polarization angle of the short flares. Each point shows the averaged polarization angle of each flare. In the case of the clockwise rotation, the rotation rate is estimated to be 1.1 ± 0.3 degree/d. The solid line in figure 7 indicates the best-fitted model of the clockwise rotation with a constant rotation rate. The rotation rate is much smaller than that in the outburst state. On the other hand, the dashed line in figure 7 indicates the model of the counterclockwise rotation. In this case, the rotation rate is estimated to be 12.1 ± 0.9 degree/d, which is relatively close to the rate in the outburst state. Hence, the two rotation episodes of the polarization vector in 3C 454.3 could have the same origin under a helical magnetic field, if the polarization angle actually rotated in the counterclockwise direction during the active state.

4.3. Estimation of the strength of the magnetic field in the emitting zone

We can estimate the strength of the magnetic field in the emitting zone using the decay timescale of observed flares. We estimate the decay timescale from flares in the active state. In figure 8, we show the light curves of flares whose timescales are of the shortest among our ob-

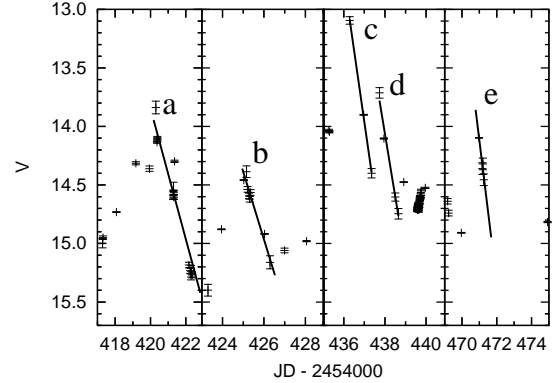


Fig. 8. V-band light curves of the short flares in the active state. The solid lines shows the best-fitted exponential decay model.

served flares. We identified five decay phases, as labeled “a”, “b”, “c”, “d” and “e” in figure 8. We calculated the decay timescale of the flares, τ_{obs} , assuming that the flux followed an exponential decay, that is, $F(t) \propto e^{-t/\tau_{\text{obs}}}$ (Böttcher et al. 2007). The decay timescales were calculated to be 1.9 ± 0.2 , 1.9 ± 0.2 , 0.89 ± 0.02 , 1.0 ± 0.1 and 0.9 ± 0.1 d for the decay phases “a”, “b”, “c”, “d” and “e” in figure 8, respectively.

We can estimate the strength of a magnetic field, B , in the emitting zone using τ_{obs} . Tashiro et al. (1995) gave the synchrotron cooling timescale, τ_s , for relativistic jets under homogeneous magnetic field, as follows:

$$\tau_s \sim 3.2 \times 10^4 \times B^{-3/2} E_{\text{ph}}^{-1/2} \delta^{-1/2} [\text{s}], \quad (1)$$

where B and δ are the strength of the magnetic field in Gauss (G) and the beaming factor δ , respectively. E_{ph} is the emitting photon energy in the observer’s frame. It is 2.25 eV in the case of our V-band observation. Following Tashiro et al. (1995), we estimated τ_s with the observed decay timescale in which the cosmological effect is corrected, to be $\tau_{\text{obs}}/(1+z)$. Using a typical beaming factor for blazars, $\delta = 20$, we calculated the strength of the magnetic field B , to be 0.14, 0.14, 0.24, 0.22 and 0.24 G from the decay phase “a”, “b”, “c”, “d” and “e”, respectively (Burbidge, Jones & Odell 1974). Thus, the estimated strength of the magnetic field using the decay timescale was typically 0.1–0.2 G.

This estimation actually provides an upper limit of B because the Compton cooling effect possibly makes τ_{obs} smaller than a real τ_s (e.g. Böttcher et al. 2007). According to Vercellone et al. (2009), the luminosity of the inverse-Compton scattering component was 10 times larger than that of the synchrotron component in 3C 454.3. This implies that a significant Compton cooling actually occurs. Hence, an accurate calculation of B requires the estimation of the Compton cooling effect through a spectral analysis including the inverse-Compton component. Observations in γ -ray range, for example, with Fermi Gamma-ray Space Telescope, are important to investigate the inverse-Compton component, and thereby,

estimate B .

The strength of the magnetic field in 3C 454.3 has been estimated to be from 0.3 to 35 G based on the spectral analysis of multi-wavelength SEDs (e.g. Ghisellini et al. 2007; Sikora, Moderski & Madejski 2008). Our estimate of the upper limit of B is smaller than those from spectral analysis. We can consider two reasons; one is that the beaming factor, δ , could be atypically smaller. If we assume an atypically small value of $\delta = 2$, B is estimated to be 0.3–0.5 G, which is consistent with typical value from spectral analysis. The other is that we may overestimate the cooling timescale τ_{obs} if the observed flares was actually a superposition of several shorter flares, and then, underestimate the upper limit of B .

5. Conclusion

We observed the outburst, faint and post-outburst active states of the blazar 3C 454.3 in 2007 in multicolor photopolarimetric mode. We found that 3C 454.3 experienced the rotations of the polarization vector in both clockwise and counterclockwise directions in the QU plane during the outburst and post-outburst active states. The feature of the bluer-when-brighter trend was observed during the outburst state. On the other hand, the feature of the redder-when-brighter trend was observed during the faint state. It indicates that the relative contribution of the thermal component increased in the V band during this state.

This work was partly supported by a Grant-in-Aid from the Ministry of Education, Culture, Sports, Science and Technology of Japan (19740104). A part of the light curve presented in this paper is based on data taken and assembled by the WEBT collaboration and stored in the WEBT archive at the Osservatorio Astronomico di Torino-INAf (<http://www.oato.inaf.it/blazars/webt/>).

References

- Bessell, M. S., Castelli, F., & Plez, B. 1998, *A&A*, 333, 231
 Böttcher, M. et al. 2007, *ApJ*, 670, 968
 Burbidge, G. R., Jones, T. W., & Odell, S. L. 1974, *ApJ*, 193, 43
 Fiorucci, M., Tosti, G., & Rizzi, N. 1998, *PASP*, 110, 105
 Fuhrmann, L., et al. 2006, *A&A*, 445, L1
 Fukugita, M., Shimasaku, K., & Ichikawa, T. 1995, *PASP*, 107, 945
 Ghisellini, G., Foschini, L., Tavecchio, F., & Pian, E. 2007, *MNRAS*, 382, L82
 González – Pérez, J. N., Kidger, M. R., & Martín – Luis, F. 2001, *AJ*, 122, 2055
 Jones, T. W., Rudnick, L., Fiedler, R. L., Aller, H. D., Aller, M. F., & Hodge, P. E. 1985, *ApJ*, 290, 627
 Larionov, V. M., et al. 2008, *A&A*, 492, L389
 Marscher, A. P., et al. 2008, *Nature*, 452, 966
 Marscher, A. P., et al. 2010, *ApJ*, 710, L126
 Miller, H. R. 1981, *ApJ*, 244, 426
 Qian, S. J., Quirrenbach, A., Witzel, A., Krichbaum, T. P., Hummel, C. A., & Zensus, J. A. 1991, *A&A*, 241, 15
 Racine, R. 1970, *ApJ*, 159, L99
 Raiteri, C. M., et al. 2007, *A&A*, 473, 819
 Raiteri, C. M., et al. 2008, *A&A*, 491, 755
 Schlegel, D. J., Finkbeiner, D. P., & Davis, M. 1998, *ApJ*, 500, 525
 Sikora, M., Moderski, R., & Madejski, G. M. 2008, *ApJ*, 675, 71
 Sillanpää, A., Takalo, L. O., Nilsson, K., & Kikuchi, S. 1993, *Ap&SS*, 206, 55
 Skrutskie, M. F., et al. 2006, *AJ*, 131, 1163
 Takahashi, T., et al. 1996, *ApJ*, 470, L89
 Tashiro, M., Makishima, K., Ohashi, T., Inada-Koide, M., Yamashita, A., Mihara, T., & Kohmura, Y. 1995, *PASJ*, 47, 131
 Urry, C. M., & Padovani, P. 1995, *PASP*, 107, 803
 Vercellone, S., et al. 2008, *ApJ*, 676, L13
 Vercellone, S., et al. 2009, *ApJ*, 690, 1018
 Villata, M., et al. 2006, *A&A*, 453, 817
 Watanabe, M., et al. 2005, *PASP*, 117, 870
 Wolff, M. J., Nordsieck, K. H. & Nook, M. A. 1996, *AJ*, 111, 856